Numerical and Theoretical Aspects of Non-Uniform Sampling of Band-Limited Images

Karlheinz Gröchenig* and Thomas Strohmer†

Abstract

This chapter presents recent developments and progress in nonuniform sampling of band-limited functions. Since the theory and practice of nonuniform sampling of 1-D signals are well understood and already treated in many articles and surveys, the emphasis will be on the nonuniform sampling of images. Both numerical, theoretical, and applied aspects of the sampling problem will be considered.

1 Introduction

The numerical processing of data, which are often given in the form of signals or images, requires always a discretization of the data by means of sampling. This means that instead of the signal or image f only its sampled values $y_i = f(x_i)$, where i runs through some index set, are stored. At the end, possibly after processing these samples, one wants to recover the original signal f from its samples. However, this is an ill-posed problem, since the subspace of functions f with $f(x_i) = y_i$ has always infinite dimension. In practical applications, signals and images are not arbitrary functions, but usually they possess some smoothness and decay properties. Usually, it is assumed that the given functions are band-limited. For band-limited functions there is

*Department of Mathematics, The University of Connecticut, Storrs, CT 06269-3009; email: groch@math.uconn.edu.

†Department of Mathematics, University of California at Davis, Davis, CA 95616-8633; email: strohmer@math.ucdavis.edu. T. Strohmer was supported by NFS grant 9973373.

an extensive theory to show how a signal or an image is well-defined by its samples and how it can be reconstructed. Moreover, it is often assumed that the signal or image is sampled uniformly on a set of the form $\alpha\mathbb{Z}$ (i.e., the set $\{\alpha k\}_{k\in\mathbb{Z}}$) or on a lattice $\alpha\mathbb{Z}^2$. This situation is well-understood and can be treated with a diligent use of the Poisson summation formula. In recent years nonuniform sampling sets appear in more and more applications. The processing of nonuniformly spaced data is required in astronomy, geophysics, medical imaging, radar, and telecommunication systems.

In this contribution we treat some recent developments in nonuniform sampling of band-limited images. Nonuniform sampling of signals in 1-D is well-understood and well documented. The reader should consult the standard references [1], [2], Chapters 3 and 4 in this book, or the SAMPTA proceedings [3] and [4] for information. Our own point of view and an efficient numerical approach are contained in [5] and in [6]. See also [7],[8],and [9].

In higher dimensions our understanding of nonuniform sampling is less complete. In this chapter we survey recent results and algorithms for nonuniform sampling in higher dimensions. The emphasis is on the numerical aspects, but we also provide theoretical results to underline the efficiency and robustness of these algorithms. Other results and methods can be found for instance in [10], [11], [12], [13], and [14].

We have adapted most of our notation to the conventions in engineering signal processing. We avoid vector notation and spell out the coordinates (x, y) of an image pixel explicitly. Therefore we discuss everything in the context of functions in 2-D. However, all results can be extended to arbitrary dimensions by a simple adjustment of the notation. We use j for the imaginary unit. A function or signal is denoted by a small letter, its Fourier transform is denoted by the corresponding capitalized letter (e.g. F is the Fourier transform of the signal f). Sometimes it is convenient to interpret matrices as vectors. This is done by simply stacking the columns of a matrix.

2 Band-Limited Images and Finite-Dimensional Models

In data processing several models of band-limited functions are in use. We discuss the traditional class of band-limited functions of two variables in $\mathbb{R}^2$, discrete band-limited images, and two-dimensional trigonometric polynomials.

2.1 Band-Limited Images

A band-limited image with spectrum in the square $[-\Omega, \Omega] \times [-\Omega, \Omega]$ is a function in $\boldsymbol{L}^2(\mathbb{R}^2)$ that can be written as

$$f(x, y) = \int_{-\Omega}^{\Omega} \int_{-\Omega}^{\Omega} F(\xi, \eta)\, e^{2\pi j(x\xi + y\eta)} d\xi d\eta\,. \tag{1}$$

Here F is the Fourier transform of f, defined as

$$F(\xi, \eta) = \int_{\mathbb{R}} \int_{\mathbb{R}} f(x, y) e^{-2\pi j(x\xi + y\eta)}\, dx dy$$

We write $\boldsymbol{B}_\Omega$ for the space of all band-limited functions of the form (1) with finite energy $\|f\|_2^2 = \int_{\mathbb{R}} \int_{\mathbb{R}} |f(x, y)|^2\, dx dy$.

Given a uniform or nonuniform sampling set $X = \{(x_i, y_i), i \in I\}$, the problem in many applications is to recover f from its samples $f(x_i, y_i), i \in I$.

In the case of uniform sampling on the lattice $\frac{1}{2\Omega}\mathbb{Z}^2 = \{(\frac{k}{2\Omega}, \frac{L}{2\Omega}), k, l \in \mathbb{Z}\}$, the higher dimensional versions of the Shannon-Whittaker-Kotel'nikov sampling theorem provide a reconstruction. Specifically,

$$f(x, y) = \sum_{k \in \mathbb{Z}} \sum_{l \in \mathbb{Z}} f\big(\frac{k}{2\Omega}, \frac{l}{2\Omega}\big) \frac{\sin 2\pi\Omega(x - \frac{k}{2\Omega}) \sin 2\pi\Omega(y - \frac{l}{2\Omega})}{\pi^2 (x - \frac{k}{2\Omega})(y - \frac{l}{2\Omega})}\,. \tag{2}$$

The so-called cardinal series is easily derived with the Poisson summation formula [15].

Sometimes other spectra are considered. This means that we consider images f for which F vanishes outside a compact set S. If f has its spectrum S in the rectangle $[-A, A] \times [-B, B]$, then the function $f(Ax, By)$ has its spectrum in $[-1, 1] \times [-1, 1]$. Similarly if the spectrum is a parallelogram, then a simple coordinate change transforms f into an image with spectrum in the square $[-1, 1] \times [-1, 1]$. Thus for most purposes it suffices to consider the sampling problem in the space $\boldsymbol{B}_\Omega$. In certain applications, in particular in problems with a radial symmetry, the spectrum is a circle (or a ball in higher dimensions).

2.2 Discrete band-limited images

For numerical implementations in real applications two new considerations have to be added: (a) One is forced to choose a finite dimensional model for images and for band-limitedness, because the numerical treatment of a linear problem must be set in a finite-dimensional vector space. (b) The number of data (samples of f) is always finite.

For this very reason reconstruction formulas like the cardinal series (2) and the large number of sampling theorems in the mathematical literature, e.g. [16], [10], [17],[18], are of limited use in practical questions.

The reduction to a finite-dimensional model is usually done by representing an image by a matrix u with entries $u(k,l), k,l = 0,\ldots,N-1$. An image has bandwidth $M < N/2$, if it can be written as

$$u(k,l) = \sum_{m=-M}^{M} \sum_{n=-M}^{M} U(m,n) e^{2\pi j(km+ln)/N} . \tag{3}$$

In this context the sampling problem asks to find a reconstruction of u from its samples $u(k_i,l_i), i = 1,\ldots,r$, where the points (k_i,l_i) are distributed nonuniformly in the square $[0,N-1] \times [0,N-1] \cap \mathbb{Z}^2$. If the sampling set is uniform, i.e., if it is a grid of the form (ak,al), then a discrete version of the Poisson summation formula yields the reconstruction formula from the samples $u(ak,al)$. See the next section, formula (7).

In this case a fast and efficient numerical reconstruction can be obtained with FFT methods. In the nonuniform case the problem is much harder, since the system matrix lacks structure.

2.3 Trigonometric Polynomials

For an analytical approach it is useful to reinterpret the representation (3) as a discretization of a trigonometric polynomial. Let

$$p(x,y) = \sum_{m=-M}^{M} \sum_{n=-M}^{M} U(m,n) e^{2\pi j(mx+ny)}$$

be the trigonometric polynomial of degree M in both the x and y-direction. Then

$$u(k,l) = p(k/N, l/N) \tag{4}$$

is just a uniformly sampled version of p. Note that p has period one in each direction. For images on a rectangle of dimension $[-A, A] \times [-B, B]$, the scaling $p(x, y) \to p(x/2A, y/2B)$ produces trigonometric polynomials with periods $2A$ and $2B$ respectively.

We will write $\boldsymbol{P}_M$ for the vector space of all trigonometric polynomials

$$p(x, y) = \sum_{m=-M}^{M} \sum_{n=-M}^{M} a(m, n) e^{2\pi j(mx+ny)} \tag{5}$$

of order M in x and in y with coefficients $a(m, n) \in \mathbb{C}$.

For the numerical analysis of the sampling problem for images, it is most convenient to regard a band-limited image on a rectangle as trigonometric polynomial in two variables, rather than as a discrete band-limited image as in (3). There are several advantages to this point of view. The discrete model is a special case of trigonometric polynomials. However, as trigonometric polynomials are functions of the continuous variables x, y, tools from mathematical analysis become available, for instance derivatives. Moreover, whereas the sampling points in the discrete model (k_i, l_i) correspond to the points $(k_i/N, l_i/N)$ in the unit square, the (nonuniform) sampling points in the continuous and periodic model are no longer restricted to be selected from a grid.

The case where the sampling points are taken from a grid (illustrated in Fig. 2.3(a)) is also called *missing data problem*, since one has to reconstruct missing samples of a discrete signal. The case where the sampling values of a continuous signal can be arbitrarily located (shown in Fig. 2.3(b)) is usually referred to as *scattered data problem*. By using trigonometric polynomials as finite-dimensional model we do not have to distinguish between these two types.

For completeness we state the regular sampling theorem for trigonometric polynomials. The following formula corresponds to the cardinal series in (2) and elucidates the Nyquist rate for $\boldsymbol{P}_M$. Let

$$D_M(x) = \frac{1}{2M+1} \sum_{k=-M}^{M} e^{2\pi jkx} = \frac{\sin(2M+1)\pi x}{(2M+1)\sin \pi x} \tag{6}$$

be the Dirichlet kernel, then for every $p \in \boldsymbol{P}_M$ we have the reconstruction

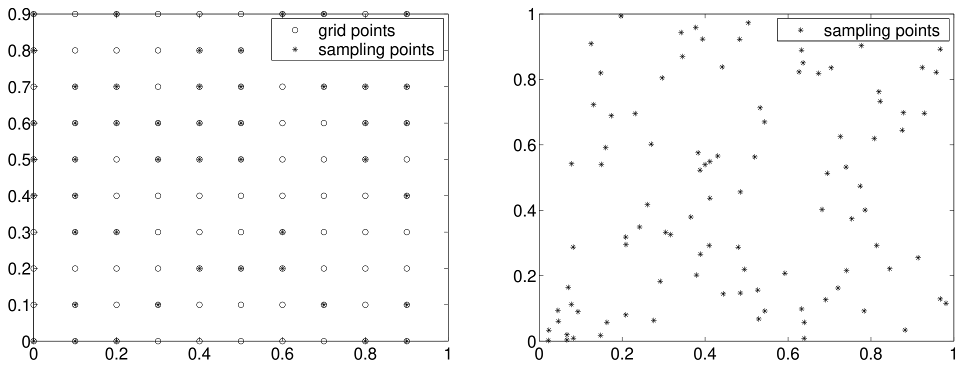

(a) Missing data (b) Scattered data

Figure 1: By using trigonometric polynomials as finite model we do not have to distinguish between the problems of missing data and scattered data

formula from the samples on the Nyquist grid $(\frac{k}{2M+1}, \frac{l}{2M+1})$

$$p(x,y) = \sum_{k=0}^{2M} \sum_{l=0}^{2M} p(\frac{k}{2M+1}, \frac{l}{2M+1}) D_M(x - \frac{k}{2M+1}) D_M(y - \frac{l}{2M+1}) \,. \tag{7}$$

Proof: We substitute (5) and the formula (6) for the Dirichlet kernel into the right-hand side of (7). To simplify the resulting expression, we use the following formula for exponential sums:

$$\frac{1}{2M+1} \sum_{k=0}^{2M} e^{2\pi jk(m-r)/(2M+1)} = \delta_{mr} \,,$$

where $\delta_{mr} = 1$ if $m = r$ and $\delta_{mr} = 0$ if $m \neq r$. We obtain

$$\begin{aligned} &\frac{1}{(2M+1)^2} \sum_{k,l=0}^{2M} \sum_{m,n=-M}^{M} a(m,n) e^{2\pi j \frac{mk+nl}{2M+1}} \sum_{r,s=-M}^{M} e^{2\pi jr(x-\frac{k}{2M+1})} e^{2\pi js(x-\frac{l}{2M+1})} \\ &= \sum_{m,n,r,s=-M}^{M} a(m,n) e^{2\pi j(rx+sy)} \left(\frac{1}{2M+1} \sum_{k=0}^{2M} e^{2\pi jk(m-r)/(2M+1)} \right) \times \end{aligned}$$

$$\times \left(\frac{1}{2M+1} \sum_{l=0}^{2M} e^{2\pi j l(n-s)/(2M+1)} \right)$$

$$= \sum_{m,n,r,s=-M}^{M} a(m,n) e^{2\pi j(rx+sy)}\, \delta_{mr}\, \delta_{ns}$$

$$= \sum_{m,n=-M}^{M} a(m,n) e^{2\pi j(mx+ny)} = p(x,y)\,,$$

as desired. ❏

3 Numerical Methods

Suppose that the samples of a trigonometric polynomial p of degree M are given at the r sampling points $(x_i, y_i), j = 1, \ldots, r$ in the unit square $[0,1] \times [0,1]$. For simplicity of notation we write $s_i := p(x_i, y_i)$ and $s = \{s_i\}_{i=1}^r$. Slightly more restrictive, the samples of a discrete signal u are given at r integer points $(k_i, l_i), i = 1, \ldots, r$, in $[0, N-1] \times [0, N-1]$.

3.1 Vandermonde Systems

Then a reconstruction of p from these samples amounts to the solution of the following system of linear equations for the unknown Fourier coefficients $a(m,n)$:

$$\sum_{m=-M}^{M} \sum_{n=-M}^{M} a(m,n) e^{2\pi j(mx_i+ny_i)} = p(x_i, y_i) = s_i \tag{8}$$

for $i = 1, \ldots, r$. These are r linear equations in the $(2M+1)^2$ unknown coefficients $a(m,n)$. From a dimension count we can deduce the following observation.

Lemma 1 *If every trigonometric polynomial $p \in \boldsymbol{P}_M$ of degree M is uniquely determined by its samples $p(x_i, y_i), i = 1, \ldots, r$, then the system matrix has full rank, and thus $r \geq (2M+1)^2$.*

In (8) the system matrix V has the entries

$$V_{i,(mn)} = e^{2\pi j(mx_i+ny_i)} \tag{9}$$

and resembles a double Vandermonde matrix. Although numerical algorithms for the solution of (ordinary) Vandermonde systems are known [19, 20], experience has shown that it is rather inefficient to solve a double Vandermonde system $Va = s$ directly.

If r is much larger than the dimension $(2M+1)^2$ of $\boldsymbol{P}_M$, then the system is over-determined. This usually causes numerical problems. On the other hand, if r is close to $(2M+1)^2$, then for general sampling sets the condition number is usually extremely large for nonuniform sampling sets, which implies unstable recovery. Condition numbers of the order $10^{10} - 10^{15}$, say, can already be observed in the case of 1-D signals [6].

At this point there is a significant difference between 1-D and higher dimensional signals. In dimension 1, a trigonometric polynomial of degree M is uniquely determined by its samples on any r distinct points, provided that $r \geq 2M+1$, consequently the system matrix has always full rank, independent of the sampling geometry. This is no longer true in higher dimensions. We will return to this problem in Section 4.

3.2 Frames in Non-Uniform Sampling

A more efficient and far-reaching approach is suggested by frame theory. Following Duffin and Schaeffer's ground breaking approach to sampling problems [16], we consider the sampled energy and compare it to the signal's true energy. The energy of $p \in \boldsymbol{P}_M$ is

$$\|p\|_2^2 = \int_0^1 \int_0^1 |p(x,y)|^2 \, dx dy = \sum_{k=-M}^{M} \sum_{l=-M}^{M} |a(k,l)|^2 \,, \tag{10}$$

whereas the sampled energy equals

$$\sum_{i=1}^{r} |p(x_i, y_i)|^2 \,.$$

For any reasonable sampling theory we need as a minimal requirement that the sampled energy is comparable to the actual energy of p. This means that there should exist positive constants $A, B > 0$, such that

$$A\|p\|_2^2 \leq \sum_{i=1}^{r} |p(x_i, y_i)|^2 \leq B\|p\|_2^2 \,. \tag{11}$$

for all trigonometric polynomials $p \in \boldsymbol{P}_M$. If the inequalities (11) are satisfied, then the set of samples $\{(x_i, y_i)\}$ is referred to as a *set of (stable) sampling* [21]. The inequality (11) is often called the *frame condition* and A and B are called the *frame bounds*.

To find an estimate for the upper bound B is usually easy and not a problem. The real challenge is to establish a positive lower bound $A > 0$. Clearly, when A is positive, then $p(x_i, y_i) = 0$ for all $i = 1, \ldots, r$, implies that $p \equiv 0$. But (11) says more: a small change of a sampled value $p(x_i, y_i)$ induces only a small change of p itself. Consequently the reconstruction of p from its samples is stable. From a numerical view point the existence of the constants A, B is not sufficient for stability, it is also required that the ratio B/A is small, i.e., the problem is well-conditioned. These observations are of fundamental importance when working with noisy data.

3.3 Toeplitz systems

In order to exploit the frame condition (11) for a numerical algorithm, we write it in terms of the coefficients $a(m, n)$ of p, rather than p itself. Substituting (5) into (11), we obtain

$$\sum_{i=1}^{r} |p(x_i, y_i)|^2 = \sum_{k,m=-M}^{M} \sum_{l,n-=-M}^{M} a(k,l)\overline{a(m,n)} \sum_{i=1}^{r} e^{2\pi j((k-m)x_i+(l-n)y_i)} . \quad (12)$$

Now collect the coefficients $a(k, l)$ into the vector a and write

$$T_{kl,mn} = \sum_{i=1}^{r} e^{-2\pi j((k-m)x_i+(l-n)y_i)} . \quad (13)$$

Then the matrix T with entries $T_{kl,mn}$, where $k, l, m, n = -M, \ldots, M$, is the system matrix of the sampling problem. Note that T acts on $\mathbb{C}^{(2M+1)^2}$. Thus by combining (12) and (13), the sampled energy can be written as

$$\sum_{i=1}^{r} |p(x_i, y_i)|^2 = \langle a, Ta \rangle \quad (14)$$

for $p \in \boldsymbol{P}_M$. By using (10) and (11), the frame inequalities turn into

$$A\|a\|_2^2 \leq \langle a, Ta \rangle \leq B\|a\|_2^2 . \quad (15)$$

Structure of T: The system matrix T has a very peculiar structure: $T_{kl,mn}$ depends only on the differences $k-m$ and $l-n$. We can rearrange T into $(2M+1)\times(2M+1)$ blocks B_{km} of size $(2M+1)\times(2M+1)$ with entries

$$(B_{km})_{ln} = T_{kl,mn} = \sum_{i=1}^{r} e^{2\pi j((k-m)x_i+(l-n)y_i)} .$$

Then each block is a Toeplitz matrix and since B_{km} depends only on $k-m$, T itself is a block Toeplitz matrix.

Using $V_{i,(mn)} = e^{2\pi j(mx_i+ny_i)}$ for the entries of the Vandermonde system (8), we calculate the entries of V^*V as

$$(V^*V)_{kl,mn} = \sum_{i=1}^{r} e^{2\pi j((m-k)x_i+(n-l)y_i)} = T_{kl,mn} ,$$

in other words,

$$T = V^*V . \tag{16}$$

This leads to an alternative approach to the system of equations (8). Instead of solving $Va = s$, we shall solve the *system of normal equations*

$$Ta = V^*Va = V^*s \tag{17}$$

for a.

In contrast to the Vandermonde type matrix V the matrix T is always a square matrix with the correct dimension $(2M+1)^2\times(2M+1)^2$, independent of the number of samples. Furthermore, numerical algorithms for Toeplitz matrices and block Toeplitz matrices are available in abundance and well-understood. This is one of the rare cases where it is advantageous to explicitly establish the system of normal equations (17) instead of staying with the naive approach in (8), since we gain structure and consequently numerical efficiency.

Spectrum of T: From (14) we see that T is always positive semi-definite. This means that the spectrum $\sigma(T)$, i.e., the set of all eigenvalues of T, is contained in $[0,\infty)$. If $(x_i,y_i), i=1,\dots,r$, is a set of stable sampling, then T is strictly positive definite and thus invertible. Furthermore, if λ_- and λ_+ denote the smallest and largest eigenvalues of T, then (14) and (15) imply that $A \leq \lambda_-$ and $\lambda_+ \leq B$, consequently $\sigma(T) \subseteq [A, B]$ and the condition number of T, defined as $\kappa(T) = \lambda_+/\lambda_-$ satisfies the estimate

$$\kappa(T) \leq B/A\,. \tag{18}$$

This means that reasonable estimates for the frame bounds A, B are of immediate relevance for the numerical behavior of the sampling problem. Estimates for condition numbers are usually a hard mathematical problem. Very few estimates for the block Toeplitz matrices in (13) are known in higher dimensions, a few of those will be discussed in Section 4.

3.4 An Efficient Reconstruction Algorithm

In almost any application the sampled values of an image come with noise. This means that we cannot be sure that the measured data s_i are actually the samples of a band-limited image, i.e., s_i is not necessarily of the form $p(x_i, y_i)$ for some trigonometric polynomial $p \in \boldsymbol{P}_M$. In this case the reconstruction of the image amounts to finding the trigonometric polynomial $p \in \boldsymbol{P}_M$ which yields the best approximation for the data s_i.

Formally, we have to solve the following *least square problem.*

$$\begin{aligned} &\text{Find } p \in \boldsymbol{P}_M\,, \text{ such that} \\ &\sum_{i=1}^{r} |p(x_i, y_i) - s_i|^2 w_i \;=\; \text{minimum in } \boldsymbol{P}_M\,. \end{aligned} \tag{19}$$

Note that, compared to the previous section, we have formulated the least squares problem in a more general fashion by introducing the weights $w_i > 0$. Such weights are useful to compensate for varying density in the sampling geometry or to fine-tune the condition number of the problem.

By increasing the bandwidth M so that $r \leq (2M + 1)^2$, one obtains an underdetermined system, and then it is usually possible to find a trigonometric polynomial $p \in \boldsymbol{P}_M$ that interpolates the data exactly as $p(x_i, y_i) = s_i$. However, in the presence of noise, such a solution is usually rough and jittery and does not seem to reproduce the image accurately. Moreover the increase of the bandwidth usually reduces the stability of the reconstruction problem. In general, it is better to stay with the original bandwidth and work with oversampling, i.e., the number of samples r is larger than the estimated bandwidth M. Then the solution to the least square problem (19) is much smoother and will resemble the original image more accurately. For an illustration of this effect see the numerical examples in Section 6.1. The choice of the appropriate bandwidth amounts to a *regularization* procedure for the sampling problem. In this sense, the solution of the least square problem can be considered as a denoising procedure. In Section 5.1 we will discuss this aspect in more detail.

We have seen that the relation (15) between the sampled energy and the block Toeplitz matrix T provides the key to the numerical solution of the nonuniform sampling problem for band-limited images [6], [22], [23]. After interpreting the formulas obtained so far in a new light, we obtain the following algorithm for the solution of the least square problem (19).

Proposition 2 *Assume that for a given sampling set* $\{(x_i, y_i), i = 1, \ldots, r\} \subseteq [0,1] \times [0,1]$ *the associated block Toeplitz matrix* T *is invertible on* $\mathbb{C}^{(2M+1)^2}$. *Furthermore, choose a set of weights* $w_i > 0$. *Then the solution to the least square problem (19) can be computed as follows.*
Step 1: Compute the entries of T *by*

$$T_{kl,mn} = \sum_{i=1}^{r} w_i e^{-2\pi j((k-m)x_i+(l-n)y_i)} \tag{20}$$

and the vector $b \in \mathbb{C}^{(2M+1)^2}$ *with coordinates*

$$b(k,l) = \sum_{i=1}^{r} w_i s_i e^{-2\pi j(kx_i+ky_i)} \tag{21}$$

for $k, l = -M, \ldots, M$.
Step 2: Compute $a_{opt} = T^{-1}b \in \mathbb{C}^{(2M+1)^2}$
Step 3: Compute the trigonometric polynomial $p_{opt} \in \boldsymbol{P}_M$ *with coefficient vector* a_{opt} *as follows:*

$$p_{opt}(x,y) = \sum_{k=M}^{M} \sum_{l=M}^{M} a_{opt}(k,l) e^{2\pi j(kx+ly)} \tag{22}$$

Then for all $p \in \boldsymbol{P}_M, p \neq p_{opt}$,

$$\sum_{i=1}^{r} |p_{opt}(x_i,y_i) - s_i|^2 w_i < \sum_{i=1}^{r} |p(x_i,y_i) - s_i|^2 w_i \tag{23}$$

Thus p_{opt} *is the unique solution to the least square problem (19).*

Proof: We have to verify inequality (19). For arbitrary $p(x,y) = \sum_{k=-M}^{M} \sum_{l=-M}^{M} a(k,l) e^{2\pi i(kx+ly)} \in \boldsymbol{P}_M$ we have

$$\sum_{i=1}^{r} |p(x_i,y_i) - s_i|^2 w_i = \tag{24}$$

$$= \sum_{i=1}^{r} |p(x_i,y_i)|^2 w_i - \sum_{i=1}^{r} (s_i \overline{p(x_i,y_i)} + \overline{s_i}\, p(x_i,y_i)) w_i + \sum_{i=1}^{r} |s_i|^2 w_i \tag{25}$$

Here the sampled energy is $\langle a, Ta \rangle$ by (14), and

$$\sum_{i=1}^{r} \overline{p(x_i,y_i)} s_i w_i = \sum_{k=-M}^{M} \sum_{l=-M}^{M} \overline{a(k,l)} \sum_{i=1}^{r} s_i e^{-2\pi j(kx_i+ly_i)} w_i = \langle b, a \rangle \, .$$

Consequently

$$\sum_{i=1}^{r} |p(x_i,y_i) - s_i|^2 = \langle a, Ta \rangle - \langle a, b \rangle - \langle b, a \rangle + \sum_{i=1}^{r} |s_i|^2 \, . \tag{26}$$

Using $Ta_{\mathrm{opt}} = b$ from Step 2 we obtain

$$\sum_{i=1}^{r} (|p(x_i,y_i) - s_i|^2 - |p_{\mathrm{opt}}(x_i,y_i) - s_i|^2) = \tag{27}$$

$$= \langle a, Ta \rangle - \langle a, b \rangle - \langle b, a \rangle - \langle a_{\mathrm{opt}}, Ta_{\mathrm{opt}} \rangle + \langle a_{\mathrm{opt}}, b \rangle + \langle b, a_{\mathrm{opt}} \rangle \tag{28}$$

$$= \langle (a - a_{\mathrm{opt}}), T(a - a_{\mathrm{opt}}) \rangle > 0 \tag{29}$$

If $a \neq a_{\mathrm{opt}}$, the last expression is strictly positive, since by hypothesis T is invertible. ❏

Proposition 2 yields an efficient reconstruction algorithm.

Algorithm 1 *Under the assumptions of Proposition 2 the solution p_{opt} can be computed in $\mathcal{O}(kM \log M + r \log(1/\varepsilon))$, where ε is a predefined tolerance, by following algorithm:*
Step 1: *Compute the entries of T and y in (20) and (21) using Beylkin's unequally spaced FFT algorithm [24]. This takes $\mathcal{O}(M \log M + r \log(1/\varepsilon))$ operations.*
Step 2: *Solve $Ta = b$ iteratively by the conjugate gradient (CG) algorithm [25]. Choose an initial guess a_0 and compute iteratively:*

$$k = 0$$

$$
\begin{aligned}
&r_0 = b - Ta_0\\
&\textbf{while } \|r_k\| > \varepsilon\|b\|\\
&k = k+1\\
&\qquad \textbf{if } k = 1\\
&\qquad\qquad q_1 = r_0\\
&\qquad \textbf{else}\\
&\qquad\qquad \beta = \|r_{k-1}\|^2/\|r_{k-2}\|^2\\
&\qquad\qquad q_k = r_{k-1} + \beta_k p_{k-1}\\
&\qquad \textbf{end}\\
&\qquad \alpha_k = \|r_{k-1}\|^2/\langle q_k, Tq_k\rangle\\
&\qquad a_k = a_{k-1} + \alpha_k q_k\\
&\qquad r_k = r_{k-1} - \alpha_k T q_k\\
&\textbf{end}\\
&a = a_k
\end{aligned}
\tag{30}
$$

The matrix-vector multiplication Tq_k above is carried out in $\mathcal{O}(M^2 \log M)$ operations via a 2-D FFT by embedding T in a block-circulant matrix [26, 27]. The solution of $Ta = b$ takes $\mathcal{O}(kM^2 \log M)$ operations, where k is the number of performed iterations.
Step 3: *If the signal is reconstructed on regularly space nodes $\{u_i, v_i\}_{i=1}^N$, the solution $p_{opt}(u_i, v_i)$ in (22) can be computed by a 2-D FFT. For nonuniformly spaced nodes we can again resort to Beylkin's USFFT algorithm.*

Alternatively to Beylkin's nonuniform FFT algorithm we can use Rokhlin's method [28]. For the extension of Rokhlin's algorithm to 2-D see [29].

Since the number of nodes at which the reconstructed signal is evaluated is usually independent of the number of given data and the bandwidth, the computational effort for the last step is not included in the operations count for the signal reconstruction.

The above algorithm is called the ACT-method in the literature. It incorporates adaptive weights (the choice of which will be discussed in the next section), the conjugate gradient method and the Toeplitz structure of the sampling problem, and seems to be one of the most efficient methods to treat the numerical aspects of nonuniform sampling.

Remarks: 1. The main problem is now to establish conditions on the sampling set under which the system matrix T is invertible. In practice, this is "almost always" the case (although the condition number may be large), but in theory this is an extremely difficult problem and far from being completely understood.

2. In dimension $d = 1$, T is invertible, if and only if $r \geq 2M+1$, i.e. if the number of samples is large enough. This follows from the fundamental theorem of algebra, according to which the polynomial $q(z) = z^M \sum_{k=-M}^{M} a_k z^k$ of degree $2M$ either has exactly $2M$ zeros counting multiplicity or is identical to 0.

3. In higher dimensions, the zero set of a trigonometric polynomial is an algebraic curve or an algebraic surface. For T to be invertible, the samples must not be contained in any algebraic surface. It is an open problem to efficiently characterize the invertibility of T. It follows from Lemma 1 that at least $(2M + 1)^2$ samples are required, but these need to be distributed appropriately. For instance, if the sampling set is contained in the straight line $\ell := \{(1/2, x''), x'' \in \mathbb{R}\}$, then the trigonometric polynomial $p(x', x'') = \sin 2\pi x'$ vanishes on ℓ and there can be no sampling theorem.

4. The number of iterations of CG depends essentially on the clustering of the eigenvalues of the system matrix [30]. If the sampling points stem from a perturbed regular sampling set, then the eigenvalues of T will be clustered around β, where β is the oversampling rate, cf. [31] and convergence will be extremely fast. Note that the Landweber-Richardson iteration (also known as frame iteration [2] or Marvasti method [1] in the sampling community) cannot take advantage of this clustering property.

5. If T is not invertible then CG converges to the minimal norm least squares solution of $Ta = b$, see [32].

3.5 Adaptive weights

Optimal performance of Algorithm 1 can be achieved by properly selecting weights w_i. A good choice for the weights originates from abstract sampling theorems in [18, 33].

To gain some motivation for the use of weights we first discuss the main factors which determine the condition number of the system matrix T.

(a) The lower bound of T is mainly determined by the large gaps in the sampling set. Suppose there is a large hole in the sampling set and choose a trigonometric polynomial $p \in \boldsymbol{P}_M$ which, like the prolate spheroidal functions, concentrates most of its energy in this hole. Then the sampling of p will not pick up any information about the main concentration of the polynomial energy. On the other hand, the samples outside that hole will be small. Consequently, the sampled energy will be small compared to the actual energy of p. For such a sampling set the lower frame bound A in the frame inequality (11) must be small. It is clear that this problem cannot be fixed by heavy oversampling outside the large gap.

Generically, large gaps and the ensuing lack of information always results in bad condition numbers. Without additional a priori information about the solution this problem cannot be fixed by any numerical method.

(b) On the other hand, clusters of sampling points within a small distance from each other will push up the upper bound B in the frame inequality, because the same local information is counted and added several times. Yet, as mentioned in (a) a cluster will not contribute much to the lower bound and to the uniqueness of the problem. In this case the condition number is large, because too much local information is given in certain areas of the image.

Problem (b) can be addressed by the *method of adaptive weights.* The idea is to compensate for the local variation of the density by using weights in the frame inequality.

We explain the idea for 1-D signals first.

Suppose that $0 \leq x_1 \leq x_2 \leq \cdots \leq x_r < 1$ is a sampling set in $[0, 1]$. Then the natural weights are defined as $w_i = (x_{i+1} - x_{i-1})/2$, here w_i is the length of the interval around the point x_i between the midpoints $(x_{i-1} + x_i)/2$ and $(x_{i+1} + x_i)/2$. Thus if many samples are clustered near a point x_i, then the weight w_i is small. If x_i is the only sampling point in a large neighborhood, then the corresponding weight is large.

Extensive numerical simulations have demonstrated that this method can improve the condition number of nonuniform sampling problems significantly [6], [27]. In our experience it should always be used with highly nonuniform sampling sets.

In higher dimensions the calculation of appropriate weights is a bit more delicate. We discuss two easy and practical choices for the weight function, namely Voronoi regions and cell counting.

(a) Given a sampling set, the *Voronoi region* V_i of a point (x_i, y_i) consists of all points which are closer to (x_i, y_i) than to any other sample. Formally

$$V_i = \{(x, y) : (x - x_i)^2 + (y - y_i)^2 \le (x - x_k)^2 + (y - y_k)^2 \text{ for all } k \ne i\} \tag{31}$$

Now let w_i be the area (volume) of the Voronoi region V_i. Clearly, the Voronoi regions for points in a cluster are small, therefore these points receive a small weight. For numerical recipes to calculate Voronoi regions consult [34], [35], [36].

(b) For the sampling problem the precise area of the Voronoi region is not crucial and often a cruder estimate for the local density is sufficient. According to the regular sampling theorem for $\boldsymbol{P}_M$ in (7) any trigonometric polynomial is uniquely determined by its samples on the grid $(\frac{k}{2M+1}, \frac{l}{2M+1}), k, l = 0, \ldots 2M$. Roughly speaking, we need one sampling point in each "Nyquist cell" $C_{kl} = [\frac{k}{2M+1}, \frac{k+1}{2M+1}] \times [\frac{l}{2M+1}, \frac{l+1}{2M+1}]$.

In the cell counting method we proceed as follows: let n_{kl} be the number of sampling points in the cell C_{kl} and set

$$w_i = \frac{1}{n_{kl}}, \qquad \text{whenever} \quad (x_i, y_i) \in C_{kl}$$

This choice of the weights guarantees that all cells contribute equally to the sampled energy.

With these choices of weights one can improve the stability and rate of convergence of the algorithm of the previous section.

Remark: 1. It is not hard to see that the invertibility of T does not depend on the choice of the weights. Let for the moment T be the matrix without using weights and T_w the matrix with weights w_i. Then $\sum_{i=1}^r |p(x_i)|^2 w_i = \langle a, T_w a\rangle = 0$ holds, if and only if $\sum_{i=1}^r |p(x_i)|^2 = \langle a, Ta\rangle = 0$. Therefore both T_w and T have the same kernel. Since a matrix is invertible, if and only if its kernel is $\{0\}$, it follows that either both T_w and T are invertible or both are singular.

2. As mentioned before, the condition number of T will be large in case of large gaps in the sampling set. Since T is of Toeplitz-type one may be tempted to use one of the many circulant preconditioners to improve upon the stability of the system. However, in the case of large gaps, preconditioning does not help, since the preconditioned problem will still have a spectral cluster at the origin, see [31].

4 Theoretical Back-Up

Even without a deeper theory, the discussed model of band-limited functions and the corresponding algorithm work remarkably well and very efficiently in numerical simulations. In this section we address some of the theoretical issues.

(a) We state a number of conditions which guarantee the invertibility of the system matrix T. These come in the form of estimates for the condition numbers of the Toeplitz matrices involved. For such estimates the use of adaptive weights is indispensable.

(b) We establish a connection between the finite-dimensional model of nonuniform sampling and the classical theory for the sampling of band-limited functions. In this way we obtain sampling theorems for band-limited images in their classical form.

For details and proofs the reader should consult the cited mathematical literature.

4.1 Condition numbers for Toeplitz systems

We start with a result for Toeplitz matrices that arose from the theory of nonuniform sampling for 1-D signals.

Assume that $0 \leq x_1 < x_2 < \cdots < x_r < 1$ are samples in $[0,1]$. To preserve periodicity, we set $x_0 = x_r - 1$ and $x_{r+1} = x_1 + 1$. Then we consider the $(2M+1) \times (2M+1)$-Toeplitz matrix T (in the strict sense) with entries

$$T_{kl} = \sum_{i=1}^{r} w_i e^{-2\pi j(k-l)x_i} \text{ for } k,l = -M, \ldots, M\,.$$

For the choice of weights w_i as explained in Section 3.5, i.e., $w_i = \frac{x_{i+1}-x_{i-1}}{2}$ for $i = 1, \ldots, r$, it is possible to derive explicit estimates for the condition number of T.

Theorem 3 ([8], Thm. 5) *Assume that* $\max_{i=1,\ldots,r}(x_{i+1} - x_i) = \delta < \frac{1}{2M}$. *Then the spectrum of T is contained in*

$$\sigma(T) \subseteq [(1-2M\delta)^2, (1+2M\delta)^2]\,, \tag{32}$$

and $\kappa(T) \leq \frac{(1+2M\delta)^2}{(1-2M\delta)^2}$ *is a worst case estimate for the condition number of T.*

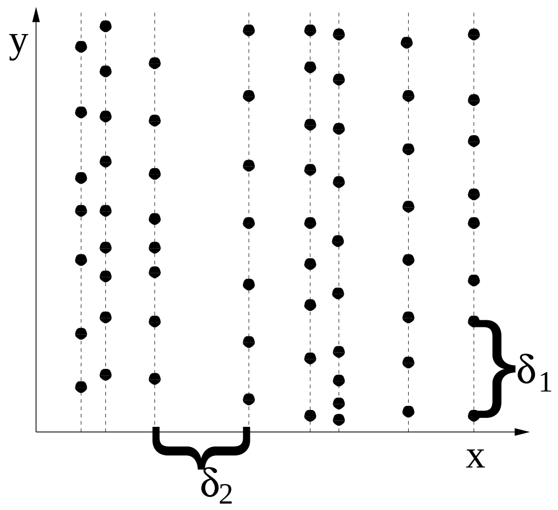

Figure 2: Line-type nonuniform sampling set, δ_1 and δ_2 denote the maximum gap in the sampling set in the y- and x-direction, respectively.

This 1-D result can be extended easily to special sampling sets and their corresponding block Toeplitz matrices in higher dimensions. In a number of applications in medical imaging and in geophysics, images are sampled line by line, but the sampling on each line is nonuniform, and the spacing between the lines is nonuniform as well. In dimension $d = 2$ such a sampling set is of the form $(x_i, y_{ik}) \in [0,1] \times [0,1], i = 1,\dots,r, k = 1,\dots,s_i$, such that $x_i < x_{i+1}$ and $y_{ik} < y_{i,k+1}$. (Again we set $x_{r+1} = x_1 + 1, x_0 = x_r - 1$ and $y_{i,0} = x_{i,s_i} - 1, y_{i,s_i+1} = y_{i,1} + 1$ to reflect the periodicity of 2-D trigonometric polynomials.) A typical example for such a sampling set is illustrated in Fig. 2.

With an appropriate choice of the adaptive weights we have the following estimates.

Theorem 4 ([23, 22]) *Suppose that* $\max_{i=1,\dots,r}(x_{i+1} - x_i) = \delta_2 < \frac{1}{2M}$ *and* $\max_{i,k\in\mathbb{Z}}(y_{i,k+1} - y_{ik}) = \delta_1 < \frac{1}{2M}$ *and choose* $w_{ik} = \frac{1}{4}(x_{i+1} - x_{i-1})(y_{i,k+1} - y_{i,k-1})$. *Then the spectrum of the block Toeplitz matrices* T *in (20) satisfies*

$$\sigma(T) \subseteq \left[(1 - 2M\delta_1)^2(1 - 2M\delta_2)^2, (1 + 2M\delta_1)^2(1 + 2M\delta_2)^2\right].$$

In particular, T *is invertible for such sampling sets with a worst case estimate* *for the condition number*

$$\kappa(T) \le \frac{(1+2M\delta_1)^2(1+2M\delta_2)^2}{(1-2M\delta_1)^2(1-2M\delta_2)^2}\,. \tag{33}$$

Note that (33) shows explicitly how, for a given sampling set, the condition number deteriorates with increasing bandwidth.

Next we state a result for arbitrary sampling sets in the unit square. Let $B_\delta(a,b) = \{(x,y) \in \mathbb{R}^2 : (x-a)^2 + (y-b)^2 < \delta^2\}$ be the disc of radius δ centered at (a,b). We say that a set $\{(x_i,y_i), i = 1,\dots,r\}$ is *δ-dense* in $[0,1]\times[0,1]$, if $\bigcup_{i=1}^r B_\delta(x_i,y_i) \supseteq [0,1]\times[0,1]$. In other words, the distance of a given sample (x_i,y_i) to its nearest neighbor $(x_k,y_k), k \neq i$ is at most 2δ.

As in Theorem 3 we choose the size of the Voronoi regions V_i as the weights and use $w_i = \text{area}\,(V_i)$ in the block Toeplitz matrix T in (20). (As in the 1-D case, the weights have to be slightly modified near the boundary of the unit square $[0,1]\times[0,1]$ to take into account the periodicity of trigonometric polynomials. To avoid additional notation, we omit these details.) Now we have the following analogue of Theorem 3 for arbitrary sampling sets in 2-D [7].

Proposition 5 *Suppose that sampling set $\{(x_i,y_i), i = 1,\dots,r\} \subseteq [0,1]\times[0,1]$ is δ-dense and*

$$\delta < \frac{\log 2}{4\pi M}\,. \tag{34}$$

Then

$$\sigma(T) \subseteq [(2-e^{4\pi M\delta})^2, 4]\,. \tag{35}$$

In particular, for arbitrary δ-dense sampling sets, the block Toeplitz matrix T is invertible and Proposition 2 and Algorithm 1 are applicable.

4.2 Towards nonuniform sampling of band-limited images

So far our main concern was an approach to the nonuniform sampling problem which emphasized the numerical solution and its practical and algorithmic aspects. In the previous section we have shown that mathematical results confirm the efficiency and feasibility of this approach. However, nonuniform sampling of trigonometric polynomials is certainly not the problem that is usually called the "irregular sampling problem of band-limited functions". This raises the question of the nature of the solutions of (8) with respect to sampling of band-limited functions in $\boldsymbol{B}_\Omega$.

For this we assume that the samples $f(x_i, y_i)$ of a band-limited function $f \in \boldsymbol{B}_\Omega$ are given on an infinite discrete (nonuniform) set $\{(x_i, y_i), i \in I\}$. (Since there is no canonical way to enumerate a nonuniform set in $\mathbb{R}^2$, we write I for the index set rather than $\mathbb{Z}$ which would suggest some order.) For simplicity we assume that $\Omega = 1/2$, i.e. $F(\xi, \eta) = 0$ for $(\xi, \eta) \notin [-1/2, 1/2] \times [-1/2, 1/2]$.

For the solution or approximate solution of this infinite-dimensional problem we argue in the style of Galerkin or finite element methods.

1. *Take just the samples in the square $[-M-1/2, M+1/2]^2$, approximate them by the samples of a trigonometric polynomial p_M of degree M and period $2M+1$.*

Except for a different normalization we have solved this problem in Section 3. Set

$$(x_i', y_i') = \left(\frac{x_i + M + 1/2}{2M+1}, \frac{y_i + M + 1/2}{2M+1}\right).$$

Since these normalized samples are in the square $[0,1] \times [0,1]$, Proposition 2 and Algorithm 1 furnish a trigonometric polynomial p of order M which minimizes the least square deviation

$$\sum_{i \in I : (x_i, y_i) \in [-M-1/2, M+1/2]^2} |p(x_i', y_i') - f(x_i, y_i)|^2 w_i = \text{ minimum in } \boldsymbol{P}_M\,. \quad (36)$$

Now set

$$p_M(x, y) = p\left(\frac{x + M + 1/2}{2M+1}, \frac{y + M + 1/2}{2M+1}\right).$$

Then $p_M(x_i, y_i) = p(x_i', y_i')$ and by (36) p_M is the best trigonometric polynomial of order M to approximate the data $f(x_i, y_i)$.

If p is defined as in (5), then we have

$$p_M(x, y) = \sum_{k=-M}^{M} \sum_{l=-M}^{M} a(k, l)(-1)^{k+l} e^{2\pi j(kx+ly)/(2M+1)}\,.$$

Consequently its (distributional) Fourier transform is

$$P_M(\xi,\eta) = \sum_{k=-M}^{M} \sum_{l=-M}^{M} a(k,l)(-1)^{k+l} \delta_{\frac{k}{2M+1}}(\xi)\delta_{\frac{l}{2M+1}}(\eta)\,, \tag{37}$$

where δ_x denotes the point measure at x. Like the original band-limited image f, P_M it has its support in $[-1/2, 1/2] \times [-1/2, 1/2]$.

This observation validates our intuition that trigonometric polynomials are the correct discretization of band-limited functions.

2. By virtue of (36), p_M is a good approximation of f on the big square $[-M-1/2, M+1/2]^2$. On the other hand, since p_M is periodic, whereas $f \in \boldsymbol{B}_{1/2}$ decays, p_M cannot approximate f outside that cube. This is not surprising, because we have only used information from within $[-M-1/2, M+1/2]^2$.

In order to understand the sampling problem for band-limited functions on $\mathbb{R}^2$, we need to investigate what happens when $M \to \infty$. Both (36) and (37) suggest that the local approximations p_M should converge to the original band-limited function f. Clearly any reasonable discretization of the sampling problem should enjoy this property.

The next result shows that this property holds indeed for the model of trigonometric polynomials. For other discretizations see [37], [31].

In order to avoid certain pathologies, we impose a mild assumption on the sampling set and the associated weights.

(1) There exists $R > 0$, such that

$$\bigcup_{i \in I} B_R(x_i, y_i) = \mathbb{R}^2, \tag{38}$$

in other words, there are no arbitrarily large "holes" in the sampling set.

(2) Let V_i be the Voronoi region around (x_i, y_i) as defined in (31) and let the weight w_i be the area (volume) of $V_i \cap B_R(x_i, y_i)$.

Sampling sets and weights satisfying these properties are called permissible.

Theorem 6 ([9, 22]) *Let $\{(x_i, y_i), i \in I\}$ be a permissible sampling set in $\mathbb{R}^2$ and $f \in \boldsymbol{B}_{1/2}$. Let T_M be the block Toeplitz matrix that intervenes in the solution of the least squares problem (36). If, for some $\alpha > 0$, $\sigma(T_M) \subseteq [\alpha, \beta]$ for all M, then*

$$\lim_{M\to\infty} \int_{[-M,M]^d} |f(x) - p_M(x)|^2 \, dx = 0$$

and also $\lim_{M\to\infty} p_M(x) = f(x)$ *uniformly on compact sets.*

This theorem possesses several distinct facets:

1. From a practical point of view it validates the use of the algorithm based on the interpolation of data by trigonometric polynomials. The approximation by trigonometric polynomials is indeed an appropriate finite-dimensional model for nonuniform sampling of multivariate band-limited functions.

2. Note that the main assumption "$\sigma(T_M) \subseteq [\alpha, \beta]$ for all M" is automatically satisfied for the following sampling sets as a consequence of Theorems 4 and Proposition 5.

(a) The sampling set has the product form (x_i, y_{ik}) with $\sup_i(x_{i+1}-x_i) < 1$ and $\sup_{i,k}(y_{i,k+1} - y_{ik}) < 1$, or

(b) If the sampling set is δ-dense, i.e., $\bigcup_{i\in I} B_\delta(x_i, y_i) = \mathbb{R}^2$ for a density δ satisfying $\delta < \frac{\log 2}{2\pi}$, then the assumptions of Theorem 6 are satisfied.

3. The block Toeplitz matrices T_M play the same role for the nonuniform sampling problem as the so-called stiffness matrices do in the theory of Galerkin method and finite elements for partial differential equations. In this completely different field, the uniform boundedness of the stiffness matrix is a well-known necessary assumption for numerical stability.

4.3 Sampling Theorems for Band-Limited Images

The numerical approach of Section 3 and the limit Theorem 6 can be turned into the more classical form of a frame inequality for $\boldsymbol{B}_{1/2}$.

Corollary 7 ([38, 9]) *Under the assumptions of Theorem 6 the frame inequality*

$$\alpha \|f\|^2 \le \sum_{i\in I} |f(x_i, y_i)|^2 w_i \le \beta \|f\|^2 \tag{39}$$

holds for all $f \in \boldsymbol{B}_{1/2}$.

Since the frame bounds α and β are related to the extremal eigenvalues of the Toeplitz matrices T_M, Theorem 6 allows to approximate the frame bounds α, β by the eigenvalues of T_M.

We conclude this section with a review of the most profound and spectacular nonuniform sampling theorem in higher dimensions. It was proved around 1963, but is essentially unknown in engineering circles. We hope that its brief discussion will lead to useful applications and further investigation of related numerical issues. Beurling's theorem is a sampling theorem for band-limited functions with frequency spectrum contained in a ball.

Let $\mathcal{E}_R = \{f \in L^2(\mathbb{R}^2 : F(\xi, \eta) = 0 \text{ for } \xi^2 + \eta^2 \geq R^2\}$

Theorem 8 ([10]) *Assume that the sampling set* $\{(x_i, y_i), i \in I\}$ *satisfies*

$$\inf_{i \neq k} (x_i - x_k)^2 + (y_i - y_k)^2 > 0$$

and

$$\bigcup_{i \in I} B_r(x_i, y_i) = \mathbb{R}^2 .$$

If

$$rR < \frac{1}{4}$$

then there exist frame bounds $A, B > 0$*, such that the frame inequalities*

$$A \int_{\mathbb{R}} \int_{\mathbb{R}} |f(x,y)|^2 \, dxdy \leq \sum_{i \in I} |f(x_i, y_i)|^2 \leq B \int_{\mathbb{R}} \int_{\mathbb{R}} |f(x,y)|^2 \, dxdy$$

holds for all $f \in \mathcal{E}_R$*.*

5 Deeper Aspects

The literature offers a variety of reconstruction algorithms for the costumer of sampling and reconstruction technology. However, in the applications of these algorithms to real world problems, one often is confronted with a number of additional difficulties.

- An algorithm may ask for certain parameters, e.g., relaxation parameters in iterative algorithms, which are not readily available or are not known a priori.
- An algorithm gives satisfactory results only for selected examples, usually of small dimension, but it may be too expensive for large-scale real world problems.
- The theoretical assumptions, such as required sampling density, under which the algorithm is guaranteed to be efficient are not fulfilled.

In this section we address some of these problems for the reconstruction algorithms of Section 3.4. In this form we answer some questions that we are frequently asked by users in signal processing and industry about these algorithms.

5.1 Band-Width Estimation – A Multi-Level Approach

Most theoretical results and numerical algorithms for reconstructing a band-limited signal from nonuniform samples require that the bandwidth is known a priori. This information, however, is often not available in practice, and thus the bandwidth enters the algorithm as a hidden parameter. Yet, a good choice of the bandwidth is crucial for any reconstruction algorithm in case of noisy data. It is intuitively clear that choosing too large a bandwidth leads to over-fit of the noise in the data, while too small a bandwidth yields a smooth solution but also to under-fit of the data. We will illustrate the importance of choosing the correct bandwidth by a reconstruction problem in medical imaging in Section 6.1. Of course, we do not want to search for the optimal bandwidth by trial-and-error methods. Hence the problem is to design a method that can reconstruct a signal from nonuniformly spaced and noisy samples without requiring a priori information about the bandwidth of the signal.

5.1.1 Idea of multi-level method

Let s_i denote an unperturbed sample and s_i^δ a perturbed sample. Here δ is the noise level given by

$$(\sum_{i=1}^{r} |s_i^\delta - s_i|^2)^{\frac{1}{2}} \le \delta \sum_{i=1}^{r} |s_i|^2 \,.$$

If the data are distorted by noise it does not make sense to ask for a solution p that satisfies $\sum_{i=1}^{r} |p(x_i, y_i) - s_i|^2 = 0$. All we should ask for is a solution p that fulfills

$$\sum_{i=1}^{r} |p(x_i, y_i) - s_i|^2 \le \delta^2 \sum_{i=1}^{r} |s_i|^2 \,. \tag{40}$$

The method we propose is based on the following idea. For simplicity of notation we represent the following approach without using weights, the resulting method can be easily modified to incorporate weights. Furthermore, Q_M denotes the orthogonal projection from $\boldsymbol{B}$ onto $\mathcal{P}_M$, and $\tau \geq 1$ is a fixed regularization parameter.

Let the noisy samples $s^\delta = \{s_i^\delta\}_{i=1}^r = \{f^\delta(x_i, y_i)\}_{i=1}^r$ of $f \in \boldsymbol{B}$ be given. We start with initial degree $M = 1$ and run Algorithm 1 until the iterates $p_{1,k}$ satisfy for the first time the *inner stopping criterion*

$$\sum_{i=1}^r |p_{1,k}(x_i, y_i) - s_i^\delta|^2 \leq 2\tau(\delta\|s^\delta\| + \|Q_1 f - f\|)\|s^\delta\| . \tag{41}$$

Denote this approximation (at iteration k_*) by p_{1,k_*}. If p_{1,k_*} satisfies the *outer stopping criterion*

$$\sum_{i=1}^r |p_{1,k_*}(x_i, y_i) - s_i^\delta|^2 \leq 2\tau\delta\|s^\delta\|^2 , \tag{42}$$

we take p_{1,k_*} as the final approximation. Otherwise we proceed to the next bandwidth $M = 2$ and run Algorithm 1 again, using p_{1,k_*} as the initial approximation by setting $p_{2,0} = p_{1,k_*}$.

In general, at level $M = N$, the inner level-dependent stopping criterion becomes

$$\sum_{i=1}^r |p_{N,k}(x_i, y_i) - s_i^\delta|^2 \leq 2\tau(\delta\|s^\delta\| + \|Q_N f - f\|)\|s^\delta\| \tag{43}$$

while the outer stopping criterion does not change since it is level-independent.

For simplicity of representation we have chosen $M = 1, 2, \ldots$ but any increasing sequence of positive integers may be chosen instead (e.g., $M = 5, 10, 15, \ldots$).

5.1.2 Stopping criteria

The reasons for the particular choice of the stopping criteria are the following. The error analysis in [39] shows that the stopping rule (43) guarantees that the iterations of the conjugate gradient algorithm are terminated before divergence of the iterates sets in. This stopping rule also ensures that CG does not iterate too long at a certain level, since if M is too small further iterations at this level will not lead to a significant improvement. Therefore we switch to the next level. The outer stopping criterion (42) controls over-fit and under-fit of the data.

As an additional problem, we note that $\|Q_N f - f\|$ cannot be computed exactly, since the solution f is not known. In [40] following recursive procedure to estimate $\|f - Q_N f\|$ has been proposed. Let us start at level $M = 1$ where $\|f - Q_1 f\|$ must be estimated. For a well-conditioned frame we estimate by using relation (7)

$$\|f - Q_1 f\|^2 \leq \|f - Q_0 f\|^2 = \|f\|^2 \approx \sum_{i=1}^{N_t} |f(x_i, y_i)|^2 w_i \,,$$

where the w_j are the weights introduced in Section 3.5. We run Algorithm 1 until the stopping criterion (41) is satisfied, at iteration k_*, say. By doing so an approximation p_{1,k_*} is obtained and we switch to the next level $M = 2$. To apply the multilevel algorithm at this level we first have to estimate $\|f - Q_2 f\|^2$. Similar to above we have that

$$\|f - Q_2 f\|^2 = \|f\|^2 - \|Q_2 f\|^2 \,.$$

We estimate as before the L^2-norm of f by the sampled norm $\|f\|^2 \approx \sum_{i=1}^{r} |f(x_i, y_i)|^2 w_i$ and we use the approximation $\|Q_2 f\|^2 \approx \|p_{1,k_*}\|^2$ to get $\|f - Q_2 f\|^2 \approx \sum_{i=1}^{r} |f(x_i, y_i)|^2 w_i - \|p_{k_*}\|^2$. Recall that $\|p_{1,k_*}\|^2$ is just the ℓ^2-norm of the sequence of coefficients which is calculated explicitly in Step 2 of Algorithm 1.

In general we estimate

$$\|f - Q_N f\|^2 \approx \sum_{i=1}^{r} |f(x_i, y_i)|^2 w_i - \|p_{N-1,k_*}\|^2 \,. \tag{44}$$

5.1.3 Computational efficiency

From the viewpoint of computational efficiency it is worth mentioning that there is a strong relationship between the block Toeplitz systems for different levels M. Let T_M and T_{M+1} denote the Toeplitz matrices at level M and level $M+1$ respectively. We adopt a similar notation for the associated right hand sides b_M and b_{M+1}. Then it is easy to see that the $(2M+1) \times (2M+1)$ matrix T_M with first column $(t_0, \ldots, t_{2M})^T$ is embedded in the $(2M+3) \times (2M+3)$

matrix T_{M+1} in the following way [23]:

$$T_{M+1} = \begin{pmatrix} t_0 & \dots & \bar{t}_{2M+2} \\ \vdots & T_M & \vdots \\ t_{2M+2} & \dots & t_0 \end{pmatrix}.$$

A similar relation holds for b_M and b_{M+1} (but of course this is not true for the solutions a_M and a_{M+1} of these systems). Thus when we switch from one level to the next level, we only have to compute a few new entries to establish the new linear system of equations.

The stopping criteria (43) and (42) are derived based on worst-case error estimates. Numerical experiments have shown that in practice both stopping criteria are somewhat pessimistic. It is usually possible to iterate longer before stagnation or divergence sets in. Extensive numerical experiments and the heuristic arguments in [32] indicate that a good choice for the inner stopping criterion is

$$\left(\sum_{i=1}^{r} |p_{N,k}(x_i, y_i) - s_i^\delta|^2 \right)^{\frac{1}{2}} \leq 2\tau(\delta + \|Q_N f - f\|)\|s^\delta\| \,, \tag{45}$$

and as outer stopping criterion we use

$$\left(\sum_{i=1}^{r} |p_{N,k}(x_i, y_i) - s_i^\delta|^2 \right)^{\frac{1}{2}} \leq \tau\delta\|s^\delta\| \,, \tag{46}$$

where the choice $\tau = 1$ is usually sufficient.

These are also the stopping criteria we will use in the Algorithm 2 below which in turn has been used for several numerical experiments presented in Section 6.

Note that the evaluation of $\sum_{i=1}^{r} |p_{N,k}(x_i, y_i) - s_i^\delta|^2$ can be carried out efficiently in $\mathcal{O}(M^2 \log M)$ operations by making use of equation (26), which reads

$$\sum_{i=1}^{r} |p(x_i, y_i) - s_i|^2 = \langle a, Ta \rangle - \langle a, b \rangle - \langle b, a \rangle + \sum_{i=1}^{r} |s_i|^2 \,.$$

It is useful to set

$$\Psi(a) := \langle a, Ta \rangle - \langle a, b \rangle - \langle b, a \rangle + \sum_{i=1}^{r} |s_i|^2 \,. \tag{47}$$

Summing up the multi-level algorithm can be described by following pseudo-code. For better readability we state the pseudo-code without utilizing estimate (44) and use $M = 0, 1, 2, \ldots$. Of course we make use of estimate (44) in the actual numerical implementation. Also it is straightforward to modify the algorithm for any increasing sequence of levels, such as $M = 2, 4, 6, \ldots$.

Algorithm 2 (Multi-level reconstruction algorithm:) *Input: Sampling points* $\{(x_i, y_i)\}_{i=1}^{r}$ *and samples* $\{s_i\}_{i=1}^{r}$ *and the noise level* δ. *Choose* τ *(e.g.,* $\tau = 1$*), set* $M = 0$ *and initialize* stop_level $= 0$, stop $= 0$.

> **while** *stop* $= 0$
>
>   **while** *stop_level* $= 0$
>
>   run Algorithm 1 to solve $T_M a_M = b_M$ with initial guess $a_{M,0} =: a_{M-1}$;
>
>   (this produces the iterates $a_{M,k}$)
>
>   **if** $\Psi(a_{M,k}) \leq 2\tau(\delta + \|Q_M f - f_{M-1}\|)^2)\|s^\delta\|$
>
>   *stop_level* $= 1$
>
> $a_M := a_{M,k}$
>
>   **end**
>
>   **end**
>
>   **if** $\Psi(a_M) \leq \tau\delta\|s^\delta\|$
>
>   *stop* $= 1$
>
>   Compute the solution p_M from a_M via formula (22)
>
>   **else**
>
> $M = M + 1$
>
>   **end**
>
> **end**

In order to use a_{M-1} as initial guess at the next level M we proceed as follows. a_{M-1} is a vector of length $(2M-1)^2$ whereas at level M we are computing with vectors of length $(2M+1)^2$. Hence we augment a_{M-1} to a vector of length $(2M+1)^2$ by adding zeros at those indices that correspond to frequencies of order M (a polynomial of degree M can be interpreted as polynomial of degree $M+N$ by adding N zero-coefficients). The definition $a_{M,0} := a_{M-1}$ in the algorithm above should be understood in this sense.

5.2 Ill-Conditioned Sampling Problems

In Section 4 we have seen several conditions on the sampling points $\{x_i, y_i\}$ under which the block Toeplitz matrix T is invertible. However, from a numerical point of view, the invertibility alone does not guarantee a stable reconstruction, since the condition number of T can still be extremely large. Therefore the solution of $Ta = b$ may be numerically unstable, and the sampling problem may still be ill-conditioned. In general this occurs when the sampling set has large gaps, which is a common situation in astronomy and geophysics.

In case of under-sampling the reconstruction problem is even ill-posed and does not have a unique solution. From a numerical point of view, an ill-posed problem is very similar to an ill-conditioned problem. Note that these instabilities of the reconstruction problem do *not* result from an inadequate discretization of the problem as it arises when using the truncated sinc matrix approach [41], [42], [43], [37], [31].

Numerical analysis offers a large arsenal of regularization techniques to deal with ill-posed or ill-conditioned problems. In the following, we discuss a few techniques which pertain to the sampling problem.

(a) For block Toeplitz matrices there exists a large number of preconditioners that could be applied to the ill-conditioned system $Ta = b$. However, in general they do not improve upon the stability of the problem because the preconditioned problem still has a spectral cluster at the origin and preconditioning will not be efficient. In [31] this behavior has been analyzed in detail for the 1-D case, the analysis for the higher-dimensional case is similar.

(b) Fortunately there are other possibilities to obtain a stabilized solution of $T_M a_M = b_M$. As explained in Section 3.5, the condition number of T_M essentially depends on the ratio of the maximal gap in the sampling set to the Nyquist rate, which in turn depends on the bandwidth of the signal. We can improve the stability of the system by adapting the bandwidth M of the approximation accordingly. Thus the parameter M serves as regularization parameter that balances stability and accuracy of the solution. This technique can be seen as a specific realization of *regularization by projection*, see Chapter 3 in [44].

(c) In addition, we can use the conjugate gradient method (CG) as regularization method for the solution of the block Toeplitz system in order to balance the approximation error and the propagated error. When solving a linear system $Ax = y$ by CG for noisy data y^δ with $\|y - y^\delta\| \leq \delta$, the following happens. Although the iterates x_k of the CG-iteration may diverge for $k \to \infty$, the error propagation remains limited in the beginning of the iteration. The quality of the approximation therefore depends on how many iterative steps can be performed before the iterates start to diverge. The goal is now to stop the iteration exactly at the point where the divergence sets in. In other words, the iteration count serves as a regularization parameter which needs to be controlled by appropriate stopping rules [45], [32]. Such a stopping rule is given by the *discrepancy principle*, which says that the iterations should be terminated when the iterates x_k satisfy for the first time

$$\|y^\delta - Ax_k\| \le \tau\delta \tag{48}$$

for fixed $\tau > 1$ (in practice $\tau = 1$ is usually sufficient). In our context this stopping rule reads as

$$\left(\sum_{i=1}^{r} |s_i^\delta - p(x_i, y_i)|^2\right)^{\frac{1}{2}} \le \tau\delta\,.$$

The multilevel method introduced in Section 5.1 combines both regularization techniques. By optimizing the level (bandwidth) and the number of iterations in each level it provides an efficient and robust regularization technique for ill-conditioned sampling problems. See Section 6 for numerical examples.

5.3 Additional Knowledge about the Signal

In many applications the physical process that generates the signal provides further information about its nature. Thus in general a signal is not only essentially band-limited, but physics predicts a certain rate of decay for the spectrum of the signal. For instance, geophysical potential fields have exponentially decaying Fourier transform. In case of ill-conditioned sampling problems this a priori knowledge can be used to improve the accuracy of the approximation. Instead of the usual regularization methods, such as Tikhonov regularization, we propose a heuristic approach that is computationally much cheaper.

Assume that the decay of the Fourier transform of f can be bounded by $|F(\omega_{,1}, \omega_2)| \le C\phi(\omega_1, \omega_2)$. Typical choices of ϕ for biomedical or geophysical signals are

$$\phi(\omega_1,\omega_2) = \begin{cases} e^{-\gamma\sqrt{\omega_1^2+\omega_2^2}} & \text{for some } \gamma > 0; \\ 1/(1+\omega_1^2+\omega_2^2)^\alpha, & \alpha \geq 0. \end{cases} \tag{49}$$

In order to take advantage of this information and to obtain an improved reconstruction, we will solve the following modified system of equations.

For a given degree (bandwidth) M and system $Ta = b$ we construct an array ϕ of dimension $(2M+1) \times (2M+1)$ by choosing e.g. one of the decay conditions in (49). For instance set $\phi(k,l) = 1/(1+k^2+l^2)$ for $k,l = -M,\ldots,M$. We interpret ϕ as vector, as usual by stacking its columns and define $D := \operatorname{diag}(\phi)$. Then the a priori information about the frequency decay can be incorporated by using one of the following two algorithms.
(i) Instead of solving $Ta = b$ we solve the problem

$$DTa = Db \tag{50}$$

which has the weighted pseudo-inverse solution

$$a^{(1)} = (DT)^+ Db$$

where $(DT)^+$ denotes the pseudo-inverse of DT [25].
(ii) Alternatively, we consider following problem:

$$TDc = b\,, \qquad a = Dc \tag{51}$$

which has the solution

$$a^{(2)} = D(TD)^+ b\,.$$

Of course, for invertible T we have $a = a^{(1)} = a^{(2)}$. However, if T is not invertible or ill-conditioned, then equations (50) and (51) lead to weighted minimal norm least squares solutions.

Algorithm 1 can be easily adapted to solve systems (50) and (51). To solve (50), for instance, we replace the conjugate gradient method applied to $Ta = b$ in Step 2 of Algorithm 1 by the preconditioned conjugate gradient method applied to $DTa = Db$ [25]. The computational effort per iteration is only slightly larger than that of Algorithm 1, since D is a diagonal matrix. However, in contrast to the intention of PCG, the purpose of introducing the matrix D is not to precondition the system, but to obtain an improved solution via incorporating a priori information about the frequency decay. The ordinary pseudo-inverse solution assigns each frequency (i.e., each coefficient in the solution a) the same weight, whereas by introducing the weight matrix D we "punish" errors corresponding to high frequencies in a stronger than errors corresponding to low frequencies.

Numerical experiments (see e.g., Section 6.2) confirm this heuristic approach. A thorough numerical analysis of the rate of convergences as well as the choice of appropriate stopping criteria for the associated CG iterations has still to be carried out.

6 Applications

In order to illustrate the performance of the proposed methods we will apply them to reconstruction problems arising in medical imaging, exploration geophysics, and digital image reconstruction.

6.1 Object boundary recovery in Echocardiography

Band-limited functions and trigonometric polynomials are certainly not suitable to model the shape of arbitrary objects. However, they are often useful in cases where an underlying stationary physical process imposes smoothness conditions of the object. Typical examples arise in medical imaging, for instance, in clinical cardiac studies. There the evaluation of cardiac function with parameters of left ventricular contractibility is an important part of an echocardiographic examination [46]. These parameters are derived by means of boundary tracing of endocardial borders of the Left Ventricle (LV).

The extraction of the boundary of the LV involves two steps, once the ultrasound image of a cross section of the LV is given, see Figs. 3(a)–(d). First an edge detection is applied to the ultrasound image to detect the boundary of the LV, see Fig. 3(c). However this procedure may be hampered by the presence of interfering biological structures (such as papillar muscles), by the unevenness of boundary contrast, and by various kinds of noise [47]. Thus the edge detection often provides only a set of nonuniformly spaced and perturbed boundary points rather than a connected boundary. Therefore in a second step the original boundary has to be recovered from the detected edge points, see Fig. 3(d). Since the shape of the Left Ventricle is definitely smooth, trigonometric polynomials are particularly well suited to model its boundary.

We denote the boundary of the left ventricle (LV) by f and parameterize it by $f(u) = (x_u, y_u)$, where x_u and y_u are the coordinates of f at "time" u in the x- and y-direction, respectively. Obviously, we can interpret f as a 1-D continuous, complex, and periodic function, where x_u represents the real part and y_u represents the imaginary part of $f(u)$. It follows from the approximation theorem of Stone-Weierstrass [48] that a continuous periodic function can be approximated uniformly by trigonometric polynomials. If f is smooth, we may safely assume that trigonometric polynomials of low degree provide a sufficiently accurate approximation.

Assume that we know only some arbitrary, perturbed points

$$s_k = (x_{u_k}, y_{u_k}) = f(u_k) + \delta_k, \qquad k = 0, \ldots, N-1$$

of f, and we want to recover f from these points. By a slight abuse of notation we interpret s_k as complex number and write

$$s_k = x_k + jy_k\,. \tag{52}$$

We relate the curve parameter u to the boundary points s_k by computing the distance between two successive points s_{k-1}, s_k via

$$u_0 = 0 = u_N \tag{53}$$
$$u_k = u_{k-1} + d_k \tag{54}$$
$$d_k = \sqrt{(x_k - x_{k-1})^2 + (y_k - y_{k-1})^2} \tag{55}$$

for $k = 1, \ldots, N-1$. Using the normalization $t_k = t_k/L$ with $L = u_{N-1} + d_N$, we force all sampling points to be in $[0, 1)$. Other choices for d_k in (52) can be found in [49] in conjunction with curve approximation using splines.

After the transformation (52)–(55) of the detected boundary points, we can use the 1-D version of Algorithm 1 (see [6]) to recover the boundary.

As already mentioned, the detected contour points are distorted by noise. (The noise level δ depends on the quality of the technical equipment and can be determined experimentally.) Therefore least squares approximation of the data points is preferable over exact interpolation. This raises the question of choosing the optimal degree of the approximating trigonometric polynomial. For the reconstruction of Fig. 3(d) we have used the 1-D version of the multi-level method proposed in Section 5.1. An alternative method was proposed in [23]. In general the multi-level method it is more stable

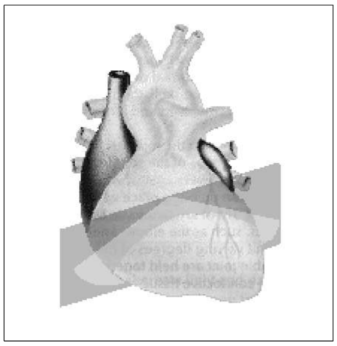

(a) 2-D echocardiography

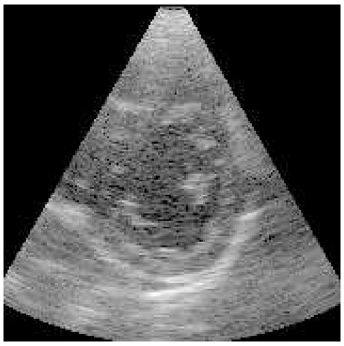

(b) Cross section of LV

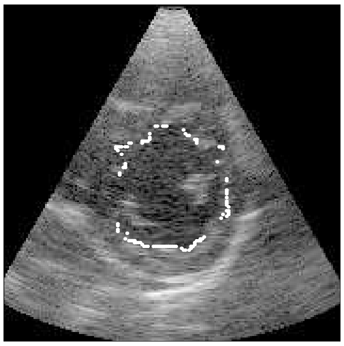

(c) Detected edge points

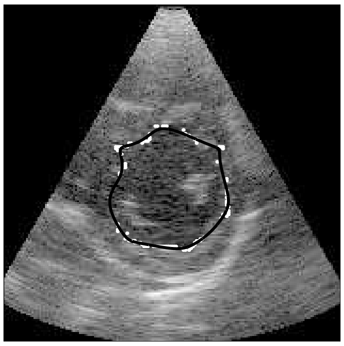

(d) Recovered boundary

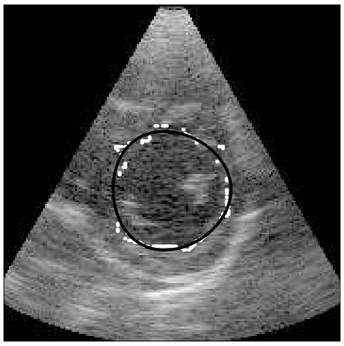

(e) Under fitted solution

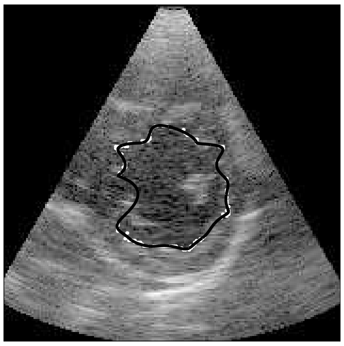

(f) Over-fitted solution

Figure 3: The recovery of the boundary of the Left Ventricle from 2-D ultrasound images is a basic step in echocardiography to extract relevant parameters of cardiac function.

and computationally only slightly more expensive than the method in [23], therefore it is preferable in practice.

Figs. 3(e)–(f) demonstrate the importance of determining an appropriate bandwidth (=degree) M for the approximating polynomial. The approximation displayed in Fig. 3(e) has been computed by applying the 1-D version of Algorithm 1, where the bandwidth M has been chosen too small. Obviously we have under-fitted the data. The over-fitted approximation was obtained by applying the same algorithm using a too large M. The result is displayed in Fig. 3(f). The approximation shown in Fig. 3(d) has been computed by the multi-level algorithm. It provides the optimal balance between fitting the data and smoothness of the solution.

6.2 Image Reconstruction in Exploration Geophysics

Exploration geophysics relies on measurements of the Earth's magnetic field with the goal of detecting anomalies which reveal underlying geological features. In geophysical practice, it is essentially impossible to gather data in a form that allows direct interpretation. Geoscientists, used to look at their measurements on maps or profiles and aim at further processing, need a representation of the originally irregularly spaced (scattered) data points on a regular grid.

Gridding is thus one of the first and crucial steps in the analysis of geophysical data. However, a number of practical constraints, such as measurement errors and the huge amount of data, make the development of reliable gridding methods a difficult task. It is agreed in the geophysics community that "a good image of the earth hides our data acquisition footprint" [50]. Unfortunately many gridding methods proposed in the literature fail in this aspect, and show how the data were sampled and processed, in particular when the data are noisy. Figs. 6.2(a)-(d) illustrate this problem for the recovery of the gravitational field from noisy scattered data.

Our synthetic anomaly represents the gravitational acceleration caused by an ensemble of buried rectangular boxes of different size, depth, and density contrast, see Fig. 6.2(b). This anomaly was sampled at a highly scattered set of 1000 sampling points. The sampling geometry is depicted in Fig. 6.2(a) together with the contour plot of the original anomaly. Note that this sampling set is composed of a line-type sampling pattern (which is characteristic for airborne or other fast-moving measurement devices), of some clusters, and of a pure random part. We chose this sampling set because it is typical for real-world settings.

Since physical measurements contains necessarily some error, we have added white noise of 5% of the ℓ^2-norm of the sampling energy. We then reconstructed the anomaly from the nonuniform samples and plotted it on a 256×256 grid with 1-m spacing.

In the numerical computation, we exploit the fact that a potential field can be modeled as an essentially band-limited function [51]. This observation allows us to use the heuristic method of Section 5.3. Since the essential bandwidth of the anomaly is not known we use the multi-level approach proposed in Section 5.1 and apply Algorithm 2 to recover the original signal.

We compare this method to the minimal curvature method [52], which is a standard reconstruction method in geophysics. The minimum curvature method produces an acceptable approximation, but – similar to splines – it does not conform to a relevant physical model. The approximation together with the sampling set is shown in Fig. 6.2(c). The error between the original anomaly and the approximation is depicted in Fig. 6.2(d). One can clearly see from Fig. 6.2(d) that there is a strong correlation between approximation error and the sampling set. The minimal curvature method is very sensible to the sampling geometry and is not able to hide the "data acquisition footprints".

Figs. 6.2(a)-(b) display the approximation of the gravitational field shown in Figs. 6.2(a)-(b) by the multi-level method. In this case, the approximation is less distorted by the noise in the data. This does not come as a big surprise since our algorithm exploits the a priori knowledge about physical properties of potential fields.

A more detailed study of this method for signal reconstruction in geophysics can be found in Rauth's thesis [53].

6.3 Reconstruction of Missing Pixels in Images

In practice images are rarely band-limited in the strict sense of definition (1). But images are often *essentially M-band-limited*, i.e. $F(n, m)$ is negligible for $|n|, |m| > M$.

Our test-image is the well-known "Lena"-image of size 512×512, see Fig. 7(a). The image is sampled at 150320 randomly spaced pixels, i.e., about 39% of pixels are lost (displayed as black pixels in Fig. 7(b)). The

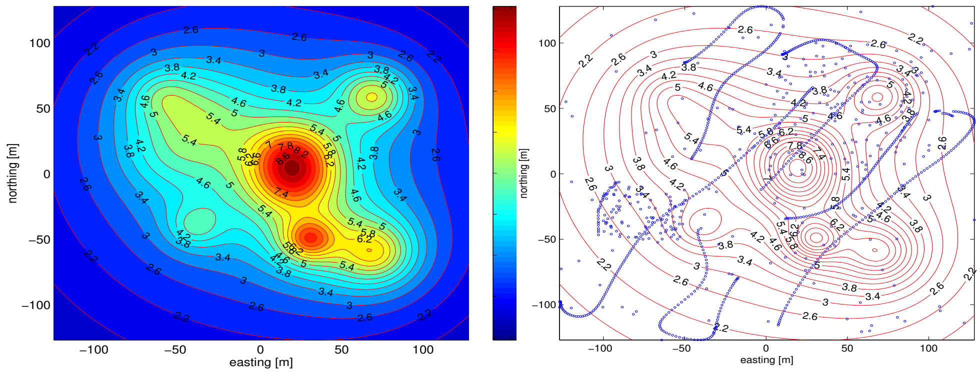

(a) Contour map of synthetic gravity anomaly, gravity is in mGal.

(b) Sampling set and synthetic gravity anomaly.

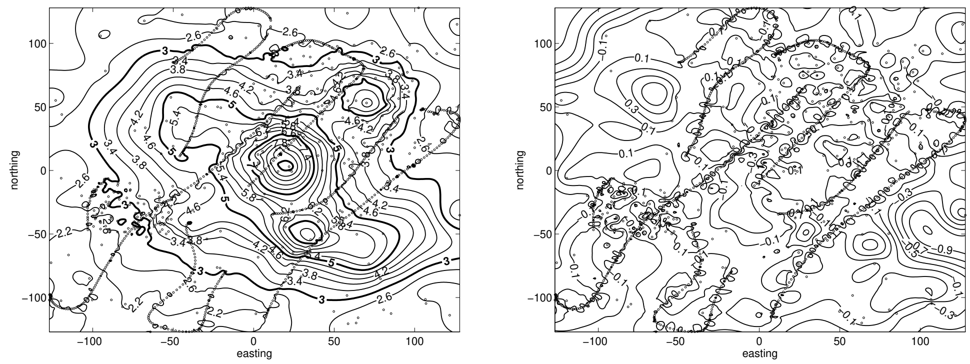

(c) Approximation from noisy samples by minimum curvature method

(d) Error between approximation and actual anomaly.

Figure 4: Many existing reconstruction methods used in exploration geophysics produce approximations that are smooth, but which do not conform to a relevant physical model. These methods are often very sensible to the sampling geometry, cf. Fig. 6.2(d).

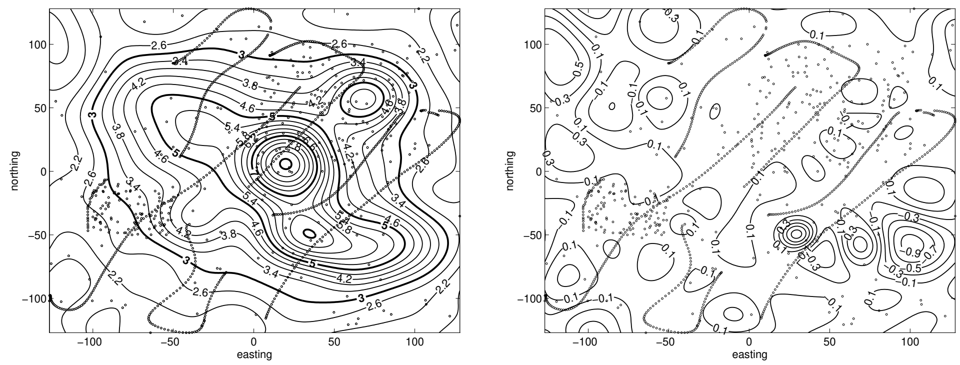

(a) Approximation from noisy samples by multi-level algorithm

(b) Error between approximation and actual anomaly.

Figure 5: The incorporation of a priori knowledge about physical properties of potential fields greatly reduced the influence of the sampling geometry, as can be seen by comparing Figs. 6.2(a) and (b) to Figs. 6.2(c) and (d).

signal-to-noise ratio is 4.04dB[1]. Since "Lena" is not band-limited, we cannot expect perfect reconstruction of the missing data.

We compare the output of Algorithm 1 (with and without using weights) to other iterative reconstruction methods proposed in the literature. These methods are the Marvasti or frame method [14, 2] and the Adaptive weights method [54]. For each method we use the same bandwidth (we set $2M+1 = 255$) and run each method until it returns a reconstruction with a signal-to-noise ratio (SNR) of at least 30dB. The results are illustrated in Fig. 6.

Marvasti's method (with optimal relaxation parameter) requires 2.88×10^9 floating point operations (*flops*) to achieve an SNR of 30dB. The Adaptive weights method needs 1.5×10^9 flops. The number of flops for Algorithm 1 (referred to as ACT in Figs. 6 and 7) is 7.99×10^8 without weights and 1.08×10^9 with Voronoi-type weights. Algorithm 1 clearly outperforms the other methods in terms of computational efficiency. Note that in case of missing data the entries of the block Toeplitz matrix used in Algorithm 1 can be easily computed by one 2-D FFT, see [27].

The bottom figure in Fig. 6 shows the rate of convergence of the re-

[1]The SNR of two images f_1, f_2 is defined as usual as $\mathrm{SNR} = 10 \log_{10}(\|f_1\|^2 / \|f_1 - f_2\|^2)$.

construction methods. In each iteration we measure the normalized least square error e_n between the original signal f and the approximation f_n via $e_n = \|f - f_n\|/\|f\|$. Also in terms of convergence rates Algorithm 1 is preferable over the other two methods. Algorithm 1 with weights gives the fastest rate of convergence, it needs only 12 iterations to achieve the required SNR of 30dB, the same algorithm without weights needs only one iteration more. The computational effort to calculate the weights and the slightly higher costs in the CG iterations due to the additional multiplication by the weights lead to a somewhat larger number of flops for the "weighted version" of Algorithm 1 in this example. The adaptive weights method needs 27 iterations and the Marvasti/frame algorithm terminates after 43 iterations.

The approximations after 15 iterations are shown in Figs. 7(c)–(f). The Marvasti or frame method [14, 2] provides an acceptable approximation of most of the lost samples, but there are still many black dots visible. The signal-to-noise ratio (SNR) after 15 iterations is 27.3dB. The adaptive weights method [54] returns an approximation with an SNR of 29.4dB. Both versions of Algorithm 1 provide a reconstruction which shows no visible difference to the original image. Other examples and more comparisons of methods can be found in [27].

The representation of edges in images requires a large bandwidth. This in turn implies that the area of missing samples has to be small in order to achieve stable reconstruction. Therefore the use of band-limited functions for the reconstruction of missing pixels is somewhat restricted. Other reconstruction methods, for instance, methods based on local Fourier bases or wavelets, have to be developed to handle the restoration of large areas of missing pixels.

References

[1] F. Marvasti, "Nonuniform sampling," in *Advanced Topics in Shannon Sampling and Interpolation Theory* (R. J. Marks II, ed.), pp. 121–156, Springer Verlag, 1993.

[2] J. Benedetto, "Irregular sampling and frames," in *Wavelets: A Tutorial in Theory and Applications* (C. K. Chui, ed.), pp. 445–507, Academic Press, 1992.

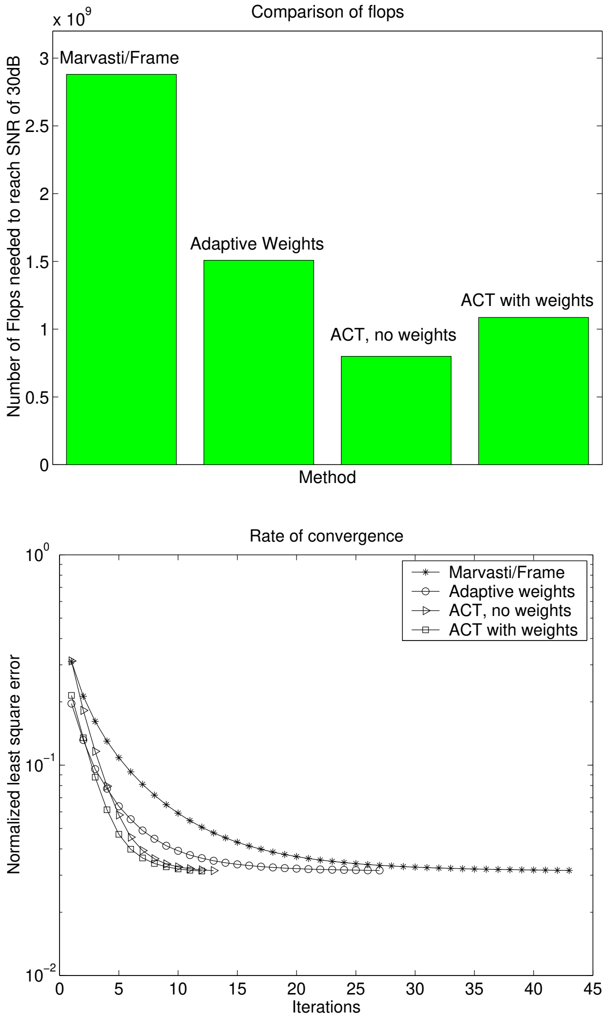

Figure 6: Comparison of flops and rates of convergence. Iterations are stopped when an SNR of 30dB is reached (which corresponds approximately to a normalized least square error of 3%). The two versions of Algorithm 1 are the most efficient methods.

(a) Lena

(b) 39 % missing samples: SNR = 4dB

(c) Marvasti/Frame: SNR = 27.3dB

(d) Adaptive weights: SNR=29.4dB

(e) ACT, no weights: SNR = 30.1dB

(f) ACT, with weights: SNR = 30.1dB

Figure 7: Nonuniformly sampled Lena and reconstructions after 15 iterations.

[3] *Proc. Sampta '95 – Workshop on Sampling Theory & Applications*, (Jurmala, Latvia), September 1995.

[4] *Proc. Sampta '97 – Workshop on Sampling Theory & Applications*, (Aveira, Portugal), June 1997.

[5] H. Feichtinger and K. Gröchenig, "Theory and practice of irregular sampling," in *Wavelets: Mathematics and Applications* (J. Benedetto and M. Frazier, eds.), pp. 305–363, CRC Press, 1994.

[6] H. G. Feichtinger, K. Gröchenig, and T. Strohmer, "Efficient numerical methods in non-uniform sampling theory," *Numerische Mathematik*, vol. 69, pp. 423–440, 1995.

[7] K. Gröchenig, "Reconstruction algorithms in irregular sampling," *Math. Comp.*, vol. 59, pp. 181–194, 1992.

[8] K. Gröchenig, "A discrete theory of irregular sampling," *Linear Algebra Appl.*, vol. 193, pp. 129–150, 1993.

[9] K. Gröchenig, "Irregular sampling, Toeplitz matrices, and the approximation of entire functions of exponential type," *Math. Comp.*, vol. 68, pp. 749–765, 1999.

[10] A. Beurling, *The collected works of Arne Beurling. Vol. 2.* Boston, MA: Birkhäuser Boston Inc., 1989. Harmonic analysis, Edited by L. Carleson, P. Malliavin, J. Neuberger and J. Wermer.

[11] K. D. Sauer and J. P. Allebach, "Iterative reconstruction of band-limited images from nonuniformly spaced samples," *IEEE Trans. CAS*, vol. 34, no. 12, pp. 1497–1506, 1987.

[12] P. L. Butzer and G. Hinsen, "Two-dimensional nonuniform sampling expansions - an iterative approach," *I, II. Appl. Anal. 32*, pp. 53–68 and 69–85, 1989.

[13] J. Benedetto and H. Wu, "A multidimensional irregular sampling algorithm and applications," in *IEEE Proc. ICASSP*, 1999.

[14] F. A. Marvasti, C. Liu, and G. Adams, "Analysis and recovery of multidimensional signals from irregular samples using nonlinear and iterative techniques," *Signal Processing*, vol. 36, pp. 13–30, 1994.

[15] D. Peterson and A. Middleton, "Sampling and reconstruction of wave-number limited functions in n-dimensional euclidean spaces," *Inform. and Contr.*, vol. 5, pp. 279–323, 1962.

[16] R. Duffin and A. Schaeffer, "A class of nonharmonic Fourier series," *Trans. Amer. Math. Soc.*, vol. 72, pp. 341–366, 1952.

[17] K. Seip, "Density theorems for sampling and interpolation in the Bargmann-Fock space," *Bull. A.M.S.*, vol. 26, pp. 322–328, 1992.

[18] H. Feichtinger and K. Gröchenig, "Non-orthogonal wavelet and Gabor expansions, and group representations," in *Wavelets and their applications* (G. Beylkin, R. Coifman, I. Daubechies, *et al.*, eds.), pp. 353–376, 20 Park Plaza, Boston, MA 02116, USA: Jones and Bartlett, 1992.

[19] L. Reichel, G. Ammar, and W. Gragg, "Discrete least squares approximation by trigonometric polynomials," *Math. Comp.*, vol. 57, pp. 273–289, 1991.

[20] C. Demeure, "Fast QR factorization of Vandermonde matrices," *Linear Algebra Appl.*, vol. 122–124, pp. 165–194, 1989.

[21] H. Landau, "Necessary density conditions for sampling and interpolation of certain entire functions," *Acta Math.*, vol. 117, pp. 37–52, 1967.

[22] K. Gröchenig, "Non-uniform sampling in higher dimensions: From trigonometric polynomials to band-limited functions," in *Modern Sampling Theory: Mathematics and Applications* (J. Benedetto and P. Ferreira, eds.), Boston: Birkhäuser, to appear.

[23] T. Strohmer, "A Levinson-Galerkin algorithm for regularized trigonometric approximation." submitted, 1998.

[24] G. Beylkin, "On the fast Fourier transform of functions with singularities," *Appl. Comp. Harm. Anal.*, vol. 2, no. 4, pp. 363–381, 1995.

[25] G. Golub and C. van Loan, *Matrix Computations, third ed.* London, Baltimore: Johns Hopkins, 1996.

[26] G. Strang, "A proposal for Toeplitz matrix calculations," *Stud. Appl. Math.*, vol. 74, pp. 171–176, 1986.

[27] T. Strohmer, "Computationally attractive reconstruction of band-limited images from irregular samples," *IEEE Trans. Image Proc.*, vol. 6, no. 4, pp. 540–548, 1997.

[28] A. Dutt and V. Rokhlin, "Fast Fourier transforms for nonequispaced data," *SIAM J. Sci. Comp.*, vol. 14, no. 6, pp. 1368–1394, 1993.

[29] A. Duijndam and M. Schonewille, "Nonuniform fast fourier transform," *Geophysics*, vol. 64, no. 2, 1999.

[30] A. van der Sluis and H. van der Vorst, "The rate of convergence of conjugate gradients," *Numer. Math.*, vol. 48, pp. 543–560, 1986.

[31] T. Strohmer, "Numerical analysis of the non-uniform sampling problem." submitted to *J. Comp. Appl. Math.*, 1999.

[32] M. Hanke, *Conjugate gradient type methods for ill-posed problems*. Harlow: Longman Scientific & Technical, 1995.

[33] H. Feichtinger and K. Gröchenig, "Gabor wavelets and the heisenberg group: Gabor expansions and short time Fourier transform from the group theoretical point of view," in *Wavelets – A Tutorial in Theory and Applications* (C. Chui, ed.), pp. 359–397, Academic Press, 1992.

[34] B. Chazelle and H. Edelsbrunner, "An improved algorithm for constructing kth-order Voronoi diagrams," *IEEE Trans. Comput.*, vol. 36, no. 11, pp. 1349–1354, 1987.

[35] A. Okabe, B. Boots, and K. Sugihara, *Spatial tessellations: concepts and applications of Voronoĭ diagrams*. Chichester: John Wiley & Sons Ltd., 1992. With a foreword by D. G. Kendall.

[36] H. G. Feichtinger and T. Strohmer, "Fast iterative reconstruction of band-limited images from irregular sampling values," in *Proc. on Computer Analysis of Images and Patterns* (D. Chetverikov and W. Kropatsch, eds.), (Budapest), pp. 82–91, Conf. CAIP, 1993.

[37] M. Harrison, *Frames and irregular sampling from a computational perspective*. PhD thesis, University of Maryland – College Park, 1998.

[38] K. Gröchenig, "Finite and infinite-dimensional models for non-uniform sampling," in *SampTA - Sampling Theory and Applications*, (Aveiro, Portugal), pp. 285–290, 1997.

[39] M. Hanke, "Regularizing properties of a truncated Newton-CG algorithm for nonlinear inverse problems," *Numer. Funct. Anal. Optim.*, vol. 18, no. 9-10, pp. 971–993, 1997.

[40] O. Scherzer and T. Strohmer, "A multi–level algorithm for the solution of moment problems," *Num.Funct.Anal.Opt.*, vol. 19, no. 3–4, pp. 353–375, 1998.

[41] D. Wingham, "The reconstruction of a band-limited function and its Fourier transform from a finite number of samples at arbitrary locations by singular value decomposition," *IEEE Trans. Circuit Theory*, vol. 40, pp. 559–570, 1992.

[42] J. Yen, "On nonuniform sampling of bandwidth-limited signals," *IRE Trans. Circuit Theory*, vol. CT-3, pp. 251–257, 1956.

[43] J. Benedetto and W. Heller, "Irregular sampling and the theory of frames, I.," *Mat. Note*, vol. 10, pp. 103–125, 1990.

[44] H. Engl, M. Hanke, and A. Neubauer, *Regularization of inverse problems.* Dordrecht: Kluwer Academic Publishers Group, 1996.

[45] A. S. Nemirovskiĭ, "Regularizing properties of the conjugate gradient method in ill-posed problems," *Zh. Vychisl. Mat. i Mat. Fiz.*, vol. 26, no. 3, pp. 332–347, 477, 1986.

[46] D. Wilson, E. Geiser, and J. Li, "Feature extraction in 2-dimensional short-axis echocardiographic images," *J. Math. Imag. Vision*, vol. 3, pp. 285–298, 1993.

[47] M. Suessner, M. Budil, T. Strohmer, M. Greher, G. Porenta, and T. Binder, "Contour detection using artifical neuronal network presegmention," in *Proc. Computers in Cardiology*, (Vienna), 1995.

[48] W. Rudin, *Fourier Analysis on Groups.* New York: Wiley Interscience, 1976.

[49] P. Dierckx, *Curve and surface fitting with splines*. Monographs on Numerical Analysis, Oxford University Press, 1993.

[50] J. Claerbout, *Geophysical Exploration Mapping*. 1998.

[51] M. Rauth and T. Strohmer, "Smooth approximation of potential fields from noisy scattered data," *Geophysics*, vol. 63, no. 1, pp. 85–94, 1998.

[52] I. Briggs, "Machine contouring using minimum curvature," *Geophysics*, vol. 39, no. 1, pp. 39–48, 1974.

[53] M. Rauth, *Gridding of geophysical potentials from noisy scattered data*. PhD thesis, University of Vienna, 1998.

[54] H. G. Feichtinger and K. Gröchenig, "Error analysis in regular and irregular sampling theory," *Applicable Analysis*, vol. 50, pp. 167–189, 1993.